J. Iron Steel Res. Int. (2022) 29:655–664
https://doi.org/10.1007/s42243-021-00633-y

ORIGINAL PAPER

Effect of yttrium treatment on alumina inclusions in high carbon steel

Yi Wang[1,2] · Chang-rong Li[1,2] · Lin-zhu Wang[1,2] · Xing-qiang Xiong[1,2] · Lu Chen[1,2]

Received: 6 February 2021 / Revised: 26 April 2021 / Accepted: 27 April 2021 / Published online: 4 August 2021

Abstract
Aluminum oxide inclusions in SWRS82B steel seriously affect the drawing performance of steel strands. The effects of different addition amounts of yttrium (within the range of 0%–0.026%) on the composition, morphology, size and spacing of aluminum oxide inclusions were studied by scanning electron microscopy and energy spectrum analysis. Based on classical thermodynamics and FactSage software, the predominance diagram of inclusions in Fe–O–S–Y system and the effect of the addition of rare earth yttrium on the stability of alumina inclusions were calculated. The results showed that molten steel was modified by adding the rare earth element yttrium. It can be inferred that the approximate route of target inclusion modification was: $Al_2O_3 \rightarrow Y_2S_3 + YAlO_3 + Al_2O_3 \rightarrow Y_2S_3 + YAlO_3 + Y_2O_2S + YAlO_3 + Al_2O_3 \rightarrow Y_2S_3 + Y_2O_2S$. The experimental samples with 0.026% added yttrium had the best inclusion characteristics, in which the inclusion surface density distribution was uniform, and the interfacial distance between inclusions was mainly in the range of 100–500 μm. After modification, the average inclusion size in molten steel was reduced by 6.9–8.6 μm. The mechanism of yttrium modification was discussed based on actual calculation results and experimental results.

Keywords Yttrium treatment · Modification of aluminum inclusions · Inclusion evolution · Thermodynamics

1 Introduction

The morphology and composition of non-metallic inclusions in steel seriously affect the quality of steel. In particular, for high carbon steel wire, in the process of wire drawing, angular non-metallic inclusions are the main cause of wire breakage, which affects all aspects of the product's performance [1–4]. In the steelmaking process, aluminum was often added to the molten steel as a deoxidizer. During the deoxidation process, the alumina inclusions easily agglomerate, forming large-size inclusions that cause the nozzle to shut off and cause industrial production to be blocked. Rare earth resources are relatively abundant. In China, the use of rare earth elements to modify non-metallic inclusions in steel has received widespread attention. Because the density of light rare earth (Ce, La) inclusions was relatively large, approximately 4.8–6.8 kg/m^2, the turbulent collision force was small, the floating force was relatively slow, and improper control can easily cause molten steel inclusions to exceed the standard [5–7]. The heavy rare earth element yttrium (Y), like light rare earth elements cerium and lanthanum (Ce, La), has strong deoxidation and desulfurization capabilities and easily generates $RE_xO_yS_z$, RE_xO_y, RE_xS_y and other high-melting point rare earth inclusions [8]. In addition, the density of the formed composite inclusions was relatively small, approximately 3.4–5.1 kg/m^2, and its floating speed was twice as fast as that of light rare earth inclusions. The solid solution strengthening effect in steel and the effect of purifying grain boundaries are obvious. It can increase the problems of water shut off [9–11].

To better study the modification of alumina inclusions by rare earth yttrium, it was necessary to further study the characteristics of inclusions and their nucleation and growth. Zhang et al. [12] studied the evolution of oxide inclusions in 18Cr–8Ni stainless steel with yttrium added during isothermal heating from 1273 to 1573 K and found that the highest transition temperature of yttrium-based oxide inclusions during heat treatment was 1373 K. Wang

✉ Chang-rong Li
cr263@163.com

[1] School of Materials and Metallurgy, Guizhou University, Guiyang 550025, Guizhou, China

[2] Guizhou Key Laboratory of Metallurgical Engineering and Process Energy Conservation, Guiyang 550025, Guizhou, China

et al. [13] studied the grain boundary characteristic distribution of yttrium with different rare earth element contents in a 90Cu10Ni alloy and found that after annealing, yttrium-rich oxysulfide inclusions help to form twin structures and large-grain clusters. Li et al. [14] studied the effect of yttrium on Al_2O_3/Al interface bonding through first principles and found that the added trace yttrium can enter the Al_2O_3/Al interface area to enhance corrosion resistance, but when the added rare earth element exceeded certain content, the effect was negative. Qiu et al. [15] studied the addition of yttrium to electroslag remelting steel, the number of inclusions was significantly reduced, and the distribution was more uniform. Fine Y–Al–O inclusions (1–2 μm) are the main inclusions in ESR-2. Liu et al. [16] found that yttrium reduced the unstable area during the hot deformation of Fe–6.5 wt.% Si alloy and significantly reduced the occurrence of microcracks. The addition of yttrium improves the ductility of the Fe–6.5 wt.% Si alloy. Kang et al. [17] found that adding an appropriate amount of yttrium (0.02 wt.%) can help reduce defects, refine grains, form a uniform microstructure and fine second phase, and improve the mechanical properties of the alloy. However, adding too much yttrium (0.2% by weight) causes element segregation, cracks and large inclusions, which reduces the mechanical properties of the alloy. Cai et al. [18] studied a Y-doped Fe–6.9 wt.% Si alloy. The average size and number of inclusions showed a similar downward trend, and the fine Y-inclusions were compared with {100} grains. The maximum interface energy may have caused the {100} grains to grow. Gerasin et al. [19] studied the substantial loss that occurs when yttrium was introduced before aluminum, mainly due to the formation of oxides. When yttrium was introduced after aluminum and calcium, yttrium was used for the precipitation of its sulfide and in this way reduced the formation of manganese sulfide.

There are many studies on the modification of inclusions using rare earth lanthanum and cerium in molten steel [20–23], but there are limited research reports on the specific process of modification of alumina inclusions by yttrium. The main purpose of this paper is to study the effect of the addition of different amounts of rare earth yttrium on the number, morphology and average size of alumina inclusions in SWRS82B steel. The experimental results were verified by thermodynamic calculations and kinetic calculations, the kinetic evolution of alumina inclusions after the addition of rare earth yttrium was analyzed, and the effectiveness of rare earth yttrium modification on alumina inclusions was determined. This study provides a reference for solving the problem of modification of alumina inclusions in high carbon steel.

2 Experimental

2.1 Experimental materials and procedures

This experiment used an intermediate frequency induction furnace and involved combining industrial pure iron (99.5%) as parent iron, recarburizer (C $\geq$ 98.5%, S $\leq$ 0.05%), and Fe–68%Mn alloy in the alumina crucible of the intermediate frequency induction furnace (170 mm OD $\times$ 150 mm ID $\times$ 280 mm HT) for melting. The crucible capacity was 20 kg. The total weight of the materials placed in the crucible in each experiment was 7 kg. When the intermediate frequency induction furnace was heated to 1873 K, the steel was stirred to completely melt the steel. After 10 min, Al bar were added for deoxidation (Al $\geq$ 98%, Si $\leq$ 0.6%, Fe $\leq$ 0.7%), and the molten steel was stirred. After 10 min, yttrium particles (purity: 99.9%) were added, and the molten steel was stirred. After five minutes, the molten steel was poured into the dried mold coated with talcum powder to cool and demold. Table 1 shows the chemical composition of the SWRS82B steel used in the experiment. The contents of carbon, silicon, manganese, phosphorus, sulfur, aluminum and yttrium were measured by inductively coupled plasma emission spectrometry, and the total oxygen content was measured by inert gas fusion pulse-infrared absorption spectroscopy.

2.2 Sample processing

The target sample (10 mm $\times$ 10 mm $\times$ 10 mm) was placed at the center of a cylindrical steel ingot by wire cutting the steel ingot, and a certain section was polished with SiC sandpaper and 1 μm diamond paste to eliminate the influence of surface roughness, and the sample surface was cleaned with ethanol. A German Zeiss ΣIGMA + X-

Table 1 Chemical composition of test steel (wt.%)

Element	C	Si	Mn	P	S	Al	O	Y
Sample S1	0.826	0.21	0.81	0.019	0.018	0.025	0.0151	0
Sample S2	0.824	0.20	0.78	0.018	0.011	0.024	0.0096	0.0079
Sample S3	0.825	0.21	0.79	0.019	0.009	0.026	0.0067	0.0140
Sample S4	0.827	0.19	0.80	0.019	0.007	0.023	0.0048	0.0260

Max20 scanning electron microscope (SEM) with energy dispersive spectrometer (EDS) was used to test the cut samples to analyse the size, morphology and chemical composition distribution of the inclusions. A scanning electron microscope was used to take 169 continuous pictures at 1000 times, corresponding to a total area of 2.6 mm × 1.755 mm. Image-ProPlus image processing software was used to analyse the characteristic distribution of inclusions on the sample surface.

3 Results and discussion

3.1 Description of inclusions size

The types of inclusions were analyzed in conjunction with the mapping pictures of typical inclusions in each sample. Scanning electron microscopic images of typical inclusions in samples S1–S4 are shown in Fig. 1. The typical inclusions of sample S1 and their spectrum scan are shown in Fig. 1a. The type of inclusions detected by SEM/EDS was alumina inclusions, and the morphology of the inclusions was more angular. The elemental distribution of the typical inclusions in sample S2 is shown in Fig. 1b, c. When the yttrium content was 0.0079%, the Al and O contents in the outer layer of typical inclusions were higher, and the Y, S and O contents in the inner layer were relatively high, indicating that Al_2O_3 inclusions were modified by yttrium to from compound inclusions. In sample S2 with an yttrium content of 0.0079%, the morphology of inclusions was still irregular, which may be due to insufficient yttrium addition. The element distribution of typical inclusions in sample S3 is shown in Fig. 1d, e. In sample S3 with 0.014% Y, the product was similar to that of sample S2, there were mainly four elements present (Al, Y, S and O), and the shape of inclusions was similar to an ellipsoid. The element distribution of typical inclusions in sample S4 is shown in Fig. 1f, g. When the amount of added yttrium was 0.026%, no composite inclusions containing Al_2O_3 were detected, and the main inclusions were Y_2S_3 and Y_2O_2S. Higher degree of spheroidization was observed in morphology of inclusions compared to samples S2 and S3. It can be concluded that without the addition of yttrium, the inclusions in the steel were mainly Al_2O_3 inclusions with large irregular shapes. To further confirm the composition of the Y–Al–O–S inclusions, the main constituent elements were homogenized. When the addition amount of yttrium was 0.0079%, the inclusions were mainly $Y_2S_3 + YAlO_3 + Al_2O_3$ composite inclusions in the steel. When the addition amount of yttrium was 0.014%, the main inclusions in the steel were composed of $Y_2S_3 + Y_2O_2S + YAlO_3 + Al_2O_3$. When the yttrium content of was 0.026%, the main inclusions in the steel were $Y_2S_3 + Y_2O_2S$ type inclusions, and the addition of yttrium had a modifying effect on the alumina inclusions. With increasing yttrium content, the transition path of inclusions was: $Al_2O_3 \rightarrow Y_2S_3 + YAlO_3 + Al_2O_3 \rightarrow Y_2S_3 + YAlO_3 + Y_2O_2S + YAlO_3 + Al_2O_3 \rightarrow Y_2S_3 + Y_2O_2S$.

SEM/EDS were used to obtain the composition content of each of the 50 inclusions in the samples S1-S4, and the transition results of the inclusions in the ternary phase diagram are shown in Fig. 2. Figure 2 shows that the inclusions generated in sample S1 did not contain yttrium because rare earth yttrium had not been added to the sample, and only alumina inclusions were present. The composite inclusions generated in sample S2 contained four elements: Al, Y, O and S. Sample S3 was similar to product sample S2, and the resulting composite inclusions contained four elements: Al, Y, O and S. The composite inclusions generated in sample S4 did not contain elemental Al, which may be due to modification by other substances.

3.2 Surface density distribution of inclusions

The pictures taken by SEM were analyzed using Image-ProPlus image processing software [24], and the data obtained for the different yttrium additions modified by alumina inclusions were integrated, as shown in Fig. 3. The areal density distribution of sample S1 is shown in Fig. 3a. The areal density distribution of inclusions ranged from 0% to 0.9%. This may be because alumina inclusions were not easy to infiltrate molten steel and were easy to aggregate forming large sizes. The inclusions produced after aluminum deoxidation quickly accumulated and floated up. Due to the influence of time, inclusions larger than 10 μm were removed, though 5–10 μm inclusions were still present in the molten steel. The areal density distribution diagrams of samples S2–S4 are shown in Fig. 3b–d. The areal density distribution range of inclusions was between 0% and 0.11%. The surface density distribution of inclusions in the sample S4 was the most uniform, which may be due to the gradual modification of alumina inclusions into the yttrium-containing rare earth inclusions. The turbulent collision force between inclusions with large differences in size increased, and the tendency of inclusions to aggregate increased. When the inclusions floated up to be removed, their distribution in the molten steel was more dispersed. The areal density distribution of sample S3 showed the second best dispersion, and the areal density distribution of sample S1 was the most uneven. The four samples were ordered by their largest areal density ratios from smallest to largest as follows: S4 < S3 < S2 < S1. After yttrium was added to the steel, it could be seen that the main factors affecting the areal density distribution of inclusions were the size of the inclusions and the force between them, and these characteristics of the inclusions are related to the

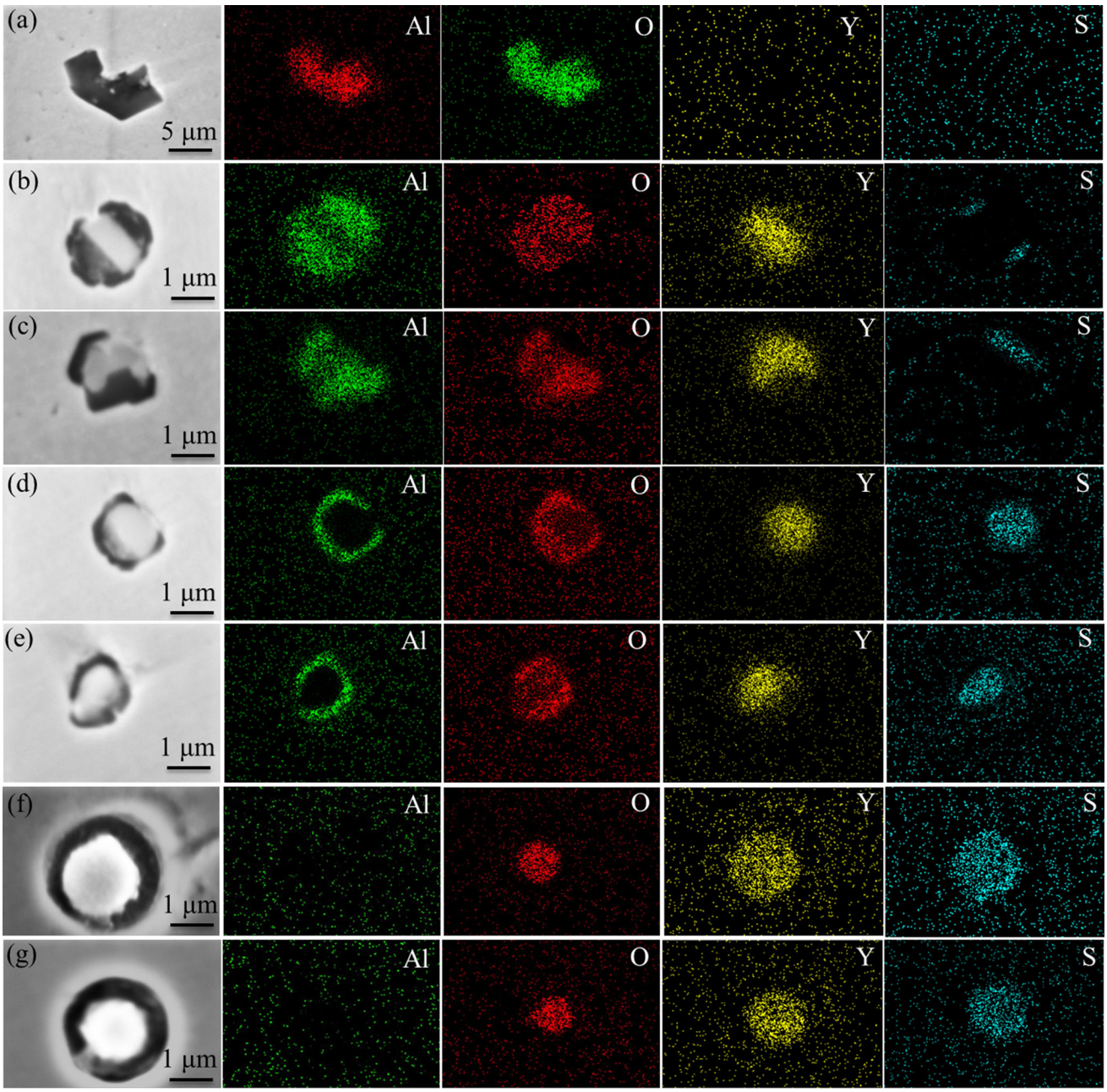

Fig. 1 SEM/EDS images of typical inclusions in samples S1–S4. **a** Sample S1; **b**, **c** sample S2; **d**, **e** sample S3; **f**, **g** sample S4

composition of the inclusions and the composition of the molten steel.

3.3 Inclusion size and interface spacing distribution

During the experiment, samples S1–S4 differed not only in the amount of yttrium added, but also in the size of the resulting inclusions. The size distribution, average size distribution and interface spacing distribution of the inclusions in samples S1–S4 are shown in Fig. 4a–c. In Fig. 4a, with the addition of rare earth yttrium, the number density of 3–5 μm inclusions was substantially reduced, the number density of 1–3 μm inclusions significantly increased, and the size distribution of inclusions became a normal distribution as a whole. These trends show that the addition of rare earth yttrium promotes the flotation of large-sized inclusions, so that only small-sized inclusions remain in the molten steel, and the effect of yttrium-modified alumina inclusions was relatively obvious. The size distribution of inclusions before and after adding rare earth yttrium is shown in Fig. 4b. When yttrium was not

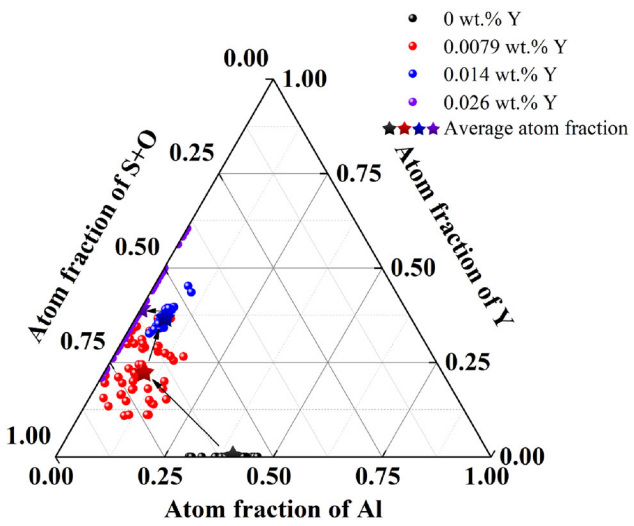

Fig. 2 Distribution diagram of inclusion elements

added, the average size of the inclusions was 8.7–10.9 μm. When the amount of yttrium added was 0.0079%, the average size of the inclusions was 2.1–2.8 μm. When the amount of yttrium added was 0.014%, the average size of the inclusions was 2.0–2.4 μm. When the amount of yttrium added was 0.026%, the average size of the inclusions was 1.8–2.3 μm, and the average size of the inclusions was the smallest, which was 6.9–8.6 μm smaller than those of sample S1. To explore the relationship between the distribution of interfacial spacing of inclusions and the amount of yttrium added, the minimum interfacial spacing between inclusions in each group of samples was calculated through data integration, as shown in Fig. 4c. In Fig. 4c, it can be seen that the interface spacing between inclusions in the sample S1 was smaller in the range of 1–10 μm, and the interface spacing between the inclusions was larger in the range of 10–100 μm. The minimum

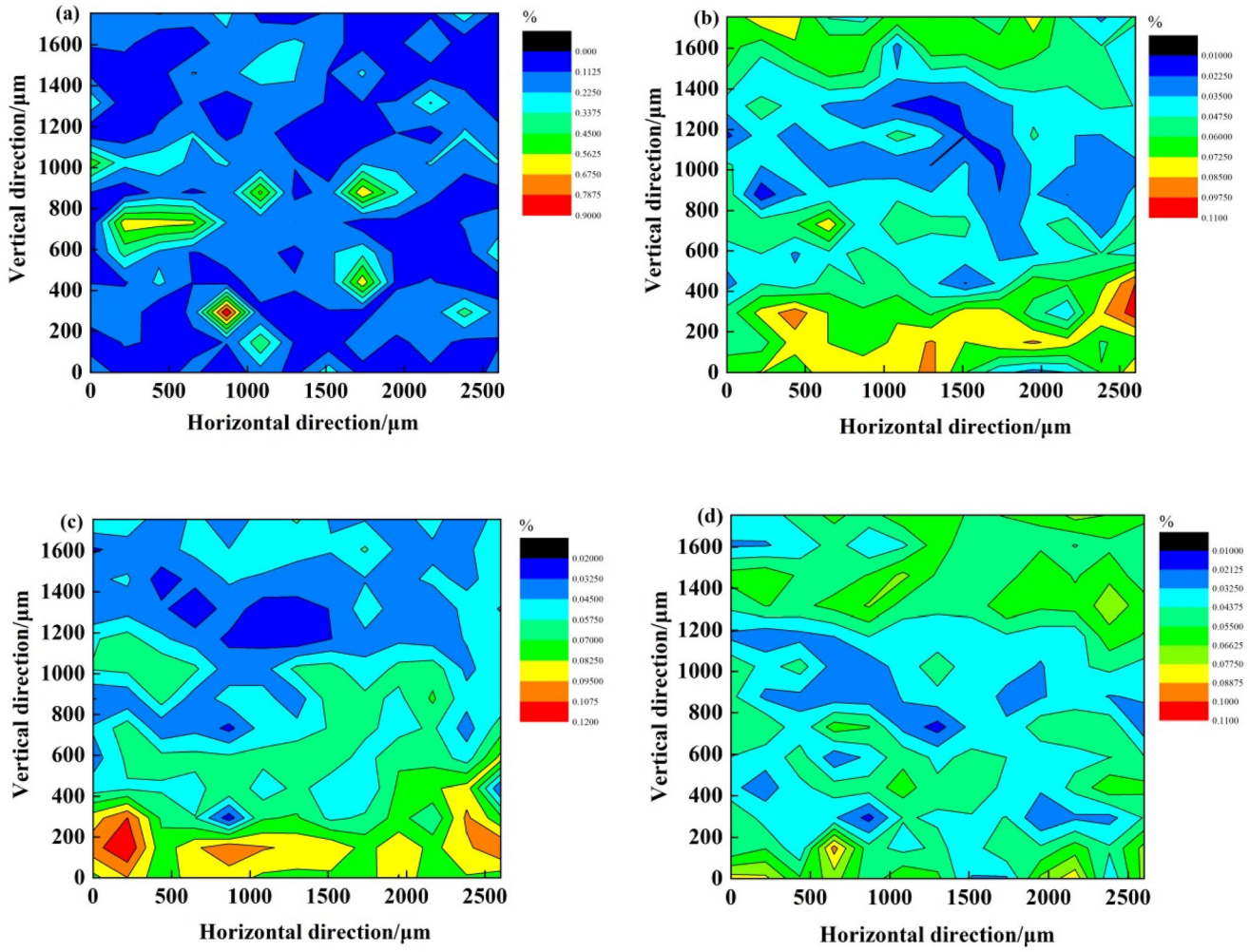

Fig. 3 Areal density distribution of alumina inclusions modified by adding different yttrium contents. **a** Sample S1; **b** sample S2; **c** sample S3; **d** sample S4

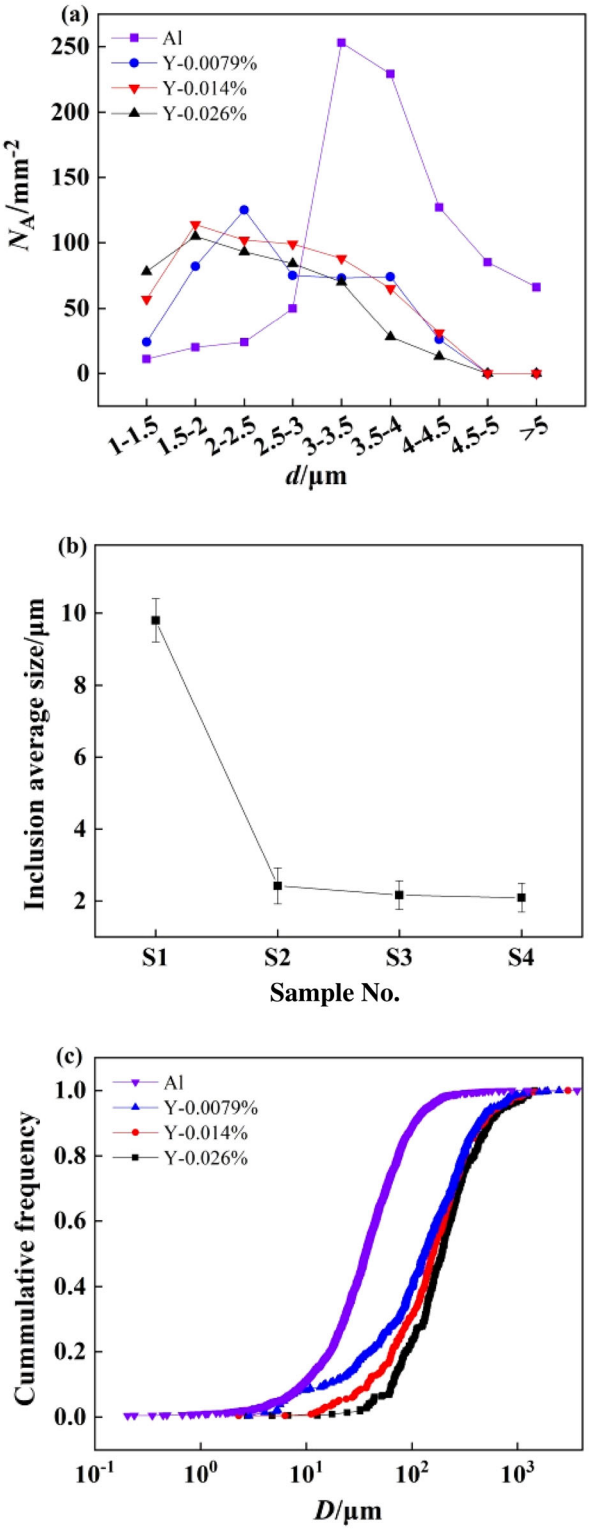

Fig. 4 Inclusion characteristic distribution. **a** Inclusion boundary size distribution; **b** inclusion size distribution; **c** inclusion boundary spacing distribution. N_A Number density of inclusions; d size of inclusions; D minimum interface distance between inclusions

interface distribution of inclusions in the samples S2–S4 was similar. Among them, the interfacial spacing between inclusions was lower in the range of 1–100 μm, and the interfacial spacing between inclusions was in the range of 100–500 μm. In the samples treated with rare earth elements, the interfacial spacing of inclusions should have increased significantly, indicating that the addition of yttrium can gradually disperse alumina inclusions in molten steel.

3.4 Thermodynamic calculation

3.4.1 Thermodynamic calculation of inclusion changes at 1873 K

To determine the mechanism that yttrium modifies alumina inclusions, the formation of inclusions should be considered in the actual reaction process. Table 2 shows the element interaction coefficients (e_i^j) of SWRS82B steel at 1873 K [25]. According to the Wagner model formula in Eq. (1), the activity coefficients of [O], [S], [Y] and [Al] elements are calculated, and then the activities are calculated according to Eq. (2). Table 3 lists the activities of [O], [S], [Y] and [Al]. Table 4 lists the transition reactions of inclusions in molten SWRS82B steel and the standard Gibbs free energy of these reactions. The correlation between the activities was calculated through Tables 3 and 4, as shown in Fig. 5. Figure 5 can predict the generation area of inclusions.

$$\lg f_i = \sum_j^n e_i^j w_j \tag{1}$$

$$a_i = f_i \cdot w_i \tag{2}$$

where f_i is the activity coefficient; n is all elements in element j; w_i and w_j represent the mass percentages of elements i and j; and a_i represents the activity of element i.

According to the composition of samples S2–S4 in Table 1, FactSage software was used to calculate the balance. Figure 6 shows the evolution of the composition of inclusions with different yttrium contents at a temperature of 1873 K. In Fig. 6a–c, with increasing yttrium content, there were three kinds of inclusions: Y_2O_3, Y_2S_3 and YS. In Fig. 6a, the weight percentages of oxygen, sulfur and aluminum were 0.0096%, 0.011% and 0.024%, respectively, for calculation. When the yttrium content was 0.0079%, Al_2O_3 and Y_2O_3 inclusions were formed. The SEM/EDS results of sample S2 in Fig. 1 should contain $YAlO_3$ inclusions. A lack of evidence of the presence of $YAlO_3$ inclusions may be caused by the absence of $YAlO_3$ inclusion data in the software database. In Fig. 6b, the weight percentages of oxygen, sulfur and aluminum were 0.0067%, 0.009% and 0.026%, respectively. When the

Table 2 Interaction coefficients of elements i and j in molten steel at 1873 K

e_i^j	C	Si	Mn	P	Al	O	S	Y
O	− 0.45	− 0.133	− 0.021	0.07	− 3.9	− 0.20	− 0.133	− 16.3
S	0.11	0.063	− 0.026	0.029	0.035	− 0.27	− 0.026	− 0.55
Y	− 0.22	–	–	–	–	− 90.7	− 7.34	− 0.006
Al	0.091	0.0056	–	–	0.045	− 6.6	0.03	–

i = O, S, Y, Al; j = C, Si, Mn, P, Al, O, S, Y

Table 3 Activities of [O], [S], [Al] and [Y] in all steels used at 1873 K

No.	$a_{[O]}$	$a_{[S]}$	$a_{[Y]}$	$a_{[Al]}$
S1	0.0045	0.0216	0	0.0238
S2	0.0022	0.0131	0.0006	0.0248
S3	0.0012	0.0107	0.0020	0.0281
S4	0.0005	0.0082	0.0056	0.0256

Table 4 Equilibrium constants used in this study [26, 27]

Reaction	ΔG^{θ}/(J mol^{-1})
$2[Al] + 3[O] = Al_2O_3(s)$	$-1{,}225{,}196 + 393.78\,T$
$2[Y] + 3[O] = Y_2O_3(s)$	$-1{,}792{,}600 + 658.0\,T$
$2[Y] + 2[O] + [S] = Y_2O_2S(s)$	$-152{,}100 + 536.0\,T$
$2[Y] + 3[S] = Y_2S_3(s)$	$-1{,}171{,}000 + 441.0\,T$
$[Y] + [S] = YS(s)$	$-321{,}080 + 91.0\,T$
$2[Y] + Al_2O_3(s) = Y_2O_3(s) + 2[Al]$	$-587{,}482 + 270.28\,T$

ΔG^{θ} Standard Gibbs free energy; T temperature

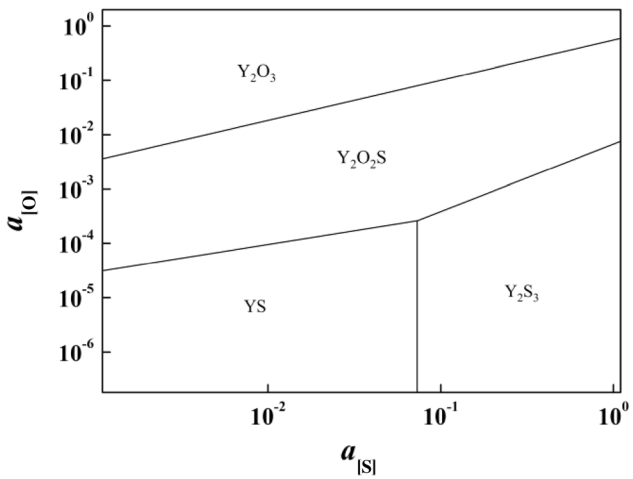

Fig. 5 Calculated inclusion stability diagram

yttrium content was 0.014%, Al_2O_3 and Y_2O_3 were formed. The SEM/EDS results of sample S3 in Fig. 1 should contain $YAlO_3$ and Y_2O_2S inclusions, but there may be an absence of data for these inclusions in the software database, and Y_2O_3 may combine with S to form Y_2O_2S inclusions. In Fig. 6c, the weight percentages of oxygen, sulfur and aluminum were 0.0048%, 0.007% and 0.023%, respectively. When the yttrium content was 0.026%, Y_2S_3 and Y_2O_3 inclusions were formed. Since there are no data for yttrium oxysulfide and yttrium aluminate in the FactSage software database, it was necessary to combine classic thermodynamic calculations to modify the conversion route of inclusions. In addition, the Gibbs free energy of the $YAlO_3$ reaction standard had not been determined, but the significance of this reaction could not be denied. Rare earth elements have commonality. Because of the existence of $LaAlO_3$ and $CeAlO_3$ inclusions, the presence of $YAlO_3$ can also be inferred and was found in the observed SEM/EDS results. Therefore, at 1873 K, in addition to the actual yttrium content in the experiment, the inclusions can be transformed according to the following route: $Al_2O_3 \rightarrow YAlO_3 + Al_2O_3 \rightarrow YAlO_3 + Y_2O_2S + YAlO_3 + Al_2O_3 \rightarrow Y_2S_3 + Y_2O_2S$.

3.4.2 Transformation of inclusions during cooling and solidification

Based on the composition of molten steel shown in Table 1, FactSage software was used to calculate the equilibrium state of different yttrium additions and the evolution of inclusion composition at different temperatures, as shown in Fig. 7. In Fig. 7a, the weight percentages of oxygen, sulfur and aluminum used in the calculation were 0.015%, 0.008% and 0.0254%, respectively. In Fig. 7b, the weight percentages of oxygen, sulfur and aluminum were 0.0096%, 0.011% and 0.024%, respectively, and were used for calculation. In Fig. 7c, the weight percentages of oxygen, sulfur and aluminum used in the calculation were 0.0067%, 0.009% and 0.026%, respectively. In Fig. 7d, the weight percentages of oxygen, sulfur and aluminum were 0.0048%, 0.007% and 0.023%,

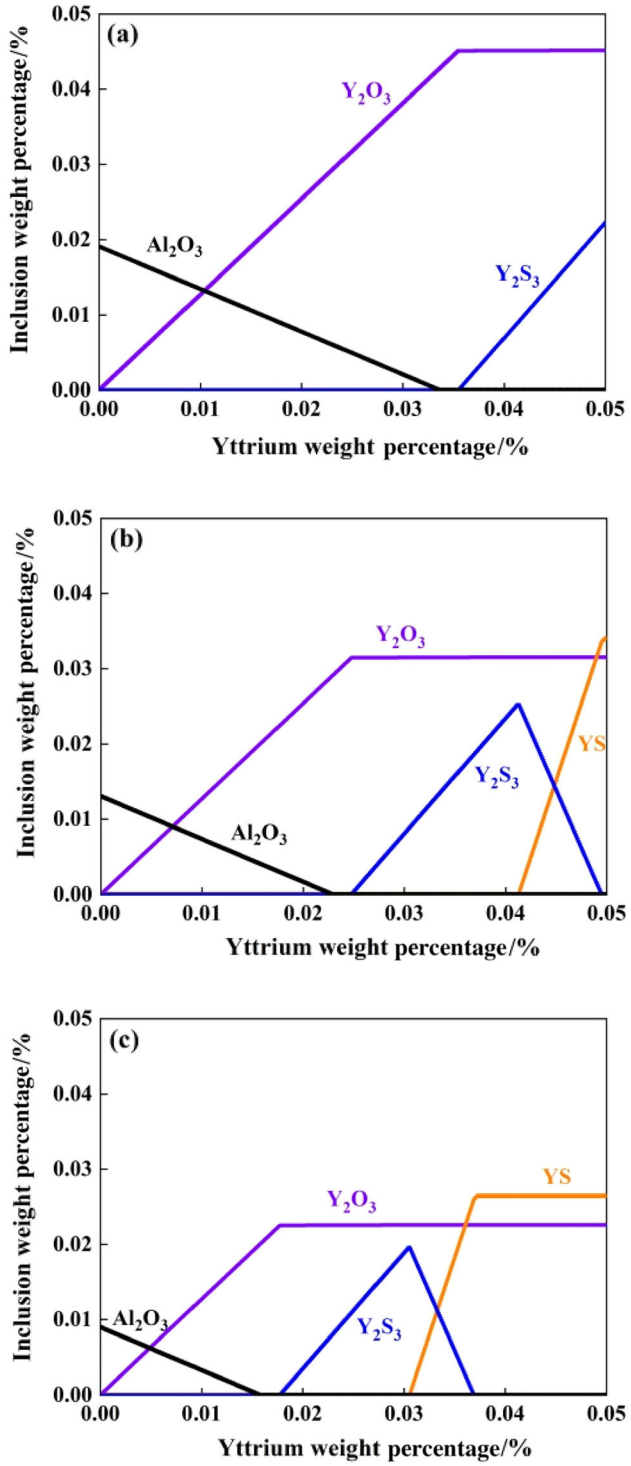

Fig. 6 Evolution of inclusion formation at 1873 K. **a** Sample S2 steel composition; **b** sample S3 steel composition; **c** sample S4 steel composition

respectively, and were used for calculation. At 1873 K, yttrium was not added to SWRS82B steel, and the inclusions were mainly composed of Al_2O_3. During the solidification of the molten steel, MnS inclusions began to precipitate at 1633 K. As shown in Fig. 7a, the reaction is described by Eqs. (3) and (4). At 1873 K, when 0.0079% yttrium was added to the steel sample, the inclusions were mainly Y_2O_3 inclusions. During the solidification of the molten steel, when the temperature was 1673 K, Y_2O_3 was partially decomposed into Y_2S_3, the original content of Y_2O_3 decreased, and MnS inclusions then began to precipitate out. Y_2O_3 disappeared completely at approximately 1673 K. During the curing process, the inclusions changed according to the following reaction: $Y_2O_3 \rightarrow Y_2S_3 + MnS$. The reaction is described by Eqs. (3)–(5), as shown in Fig. 7b. At 1873 K, when 0.014% yttrium was added to the steel sample, the inclusions were mainly composed of Y_2O_3 and Al_2O_3. When the temperature was 1673 K, the concentration of Y_2O_3 decomposed into Y_2S_3 and Al_2O_3 while the original content of Y_2O_3 decreased and the content of Y_2S_3 and Al_2O_3 increased. When Y_2O_3 dropped to 1573 K, its content completely disappeared, at this time manganese sulfide began to precipitate out. During the solidification process, the inclusions transformed in the following way: $Y_2O_3 + Al_2O_3 \rightarrow Al_2O_3 + Y_2S_3 + MnS$, and this reaction was described by Eqs. (3)–(6), as shown in Fig. 7c. At 1873 K, when 0.026% yttrium was added to the steel sample, the inclusions were mainly composed of Y_2O_3 and Y_2S_3. At approximately 1623 K, Y_2S_3 and Al_2O_3 inclusions began to precipitate out continuously, and the Y_2O_3 inclusion content dropped to 1323 K and disappeared completely. During the curing process, the inclusions were transformed according to the following route: $Y_2O_3 + Y_2S_3 \rightarrow Y_2S_3 + Al_2O_3$, and this reaction was described by Eqs. (3)–(6), as shown in Fig. 7d. Because the FactSage database is not complete, some products cannot be determined, but the above reactions still provide a useful guidance to describe the formation of inclusions. It can also be seen in Fig. 7a–d that the content of the MnS inclusions continued to decrease until it disappeared completely in Fig. 7d, indicating that the addition of yttrium not only has a better modification effect on Al_2O_3 but also has a certain modification effect on MnS inclusions.

$$2[Al] + 3[O] = Al_2O_3(s) \quad (3)$$

$$[Mn] + [S] = MnS \quad (4)$$

$$2[Y] + 3[S] = Y_2S_3(s) \quad (5)$$

$$Y_2O_3(s) = 2[Y] + 3[O] \quad (6)$$

3.5 Inclusion evolution model

Based on the analysis of the relevant results in Figs. 1, 4 and 7, the evolution of inclusions [28] can be roughly divided into three ways according to different yttrium

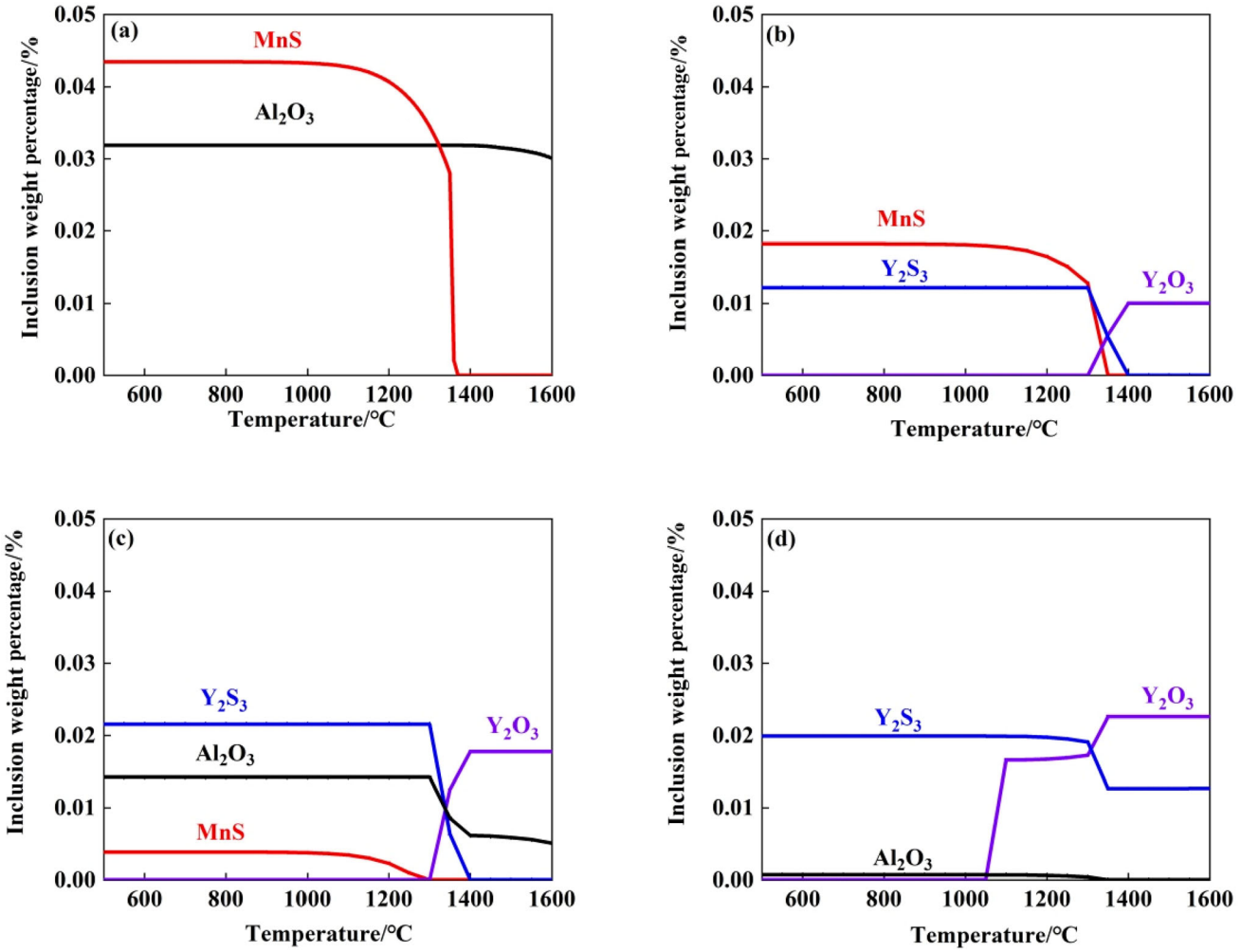

Fig. 7 Transformation of inclusions during cooling and solidification. **a** Effect of cerium addition on inclusions, w_Y = 0%; **b** effect of cerium addition on inclusions, w_Y = 0.0079%; **c** effect of cerium addition on inclusions, w_Y = 0.014%; **d** effect of cerium addition on inclusions, w_Y = 0.026%

additions, as shown in Fig. 8. When the yttrium addition amount is 0.0079%, the outer layer of inclusions at 1873 K mainly comprises Al_2O_3 inclusions, and the inside layer mainly comprises $YAlO_3$ inclusions. During the curing process, the outer layer precipitates Y_2S_3. When the yttrium addition amount is 0.014%, the outer layer of inclusions at 1873 K was mainly composed of $YAlO_3$ inclusions, and the inside contains mainly Y_2O_2S inclusions. During the curing process, the outer layer exhibits Y_2S_3 precipitates. When the amount of yttrium added is 0.026%, the outer layer of inclusions at 1873 K contains mainly Y_2S_3 inclusions, and the inside contains mainly Y_2O_2S inclusions. During the curing process, the outer layer of Y_2S_3 increases. By observing zone I and zone II longitudinally, it is found that the size of the inclusions gradually decreases, the morphology of the inclusions gradually tends to be spherical, and the edges and corners gradually become sharp. This may be because the reaction

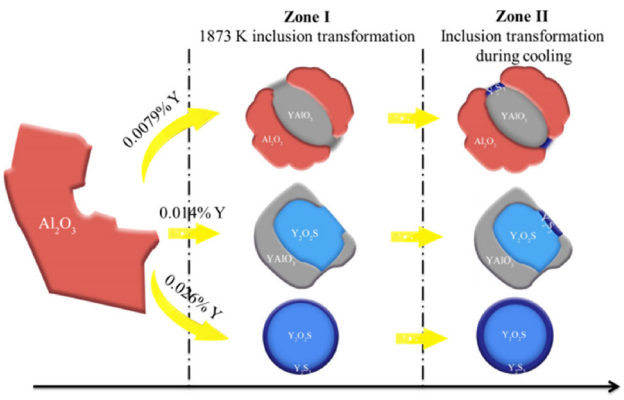

Fig. 8 Evolution model of alumina inclusions with different yttrium contents

is relatively complete, and the reactants have transformed into other substances. The collision aggregation between inclusions is dominated by Stokes collision, which directly

affects the floating of inclusions, and the formation of Y_2S_3 during the curing process is included. Compared with Al_2O_3 inclusions, the average size of composite inclusions in sample S4 is reduced by 6.9–8.6 μm. The fine dispersion effect is best. Therefore, the evolution mechanism of inclusions at high temperature is considered to combine the internal transformation of inclusions and the interface reaction between the inclusions and the steel matrix.

4 Conclusions

1. Before yttrium was added, the surface density of the sample containing aluminum inclusions accounted for the largest proportion. With increase in yttrium addition, the proportion of the maximum areal density of inclusions decreased successively. The proportion of the four samples according to the maximum areal density from small to large was as follows: S4 < S3 < S2 < S1.
2. With the addition of rare earth yttrium, the numerical density of 3–5 μm inclusions was significantly reduced, and the density of the number of 1–3 μm inclusions was significantly increased. Before yttrium was added, the interfacial spacing between inclusions was mainly in the range of 10–100 m. With the addition of yttrium, the interfacial spacing between inclusions was mainly in the range of 100–500 μm.
3. The classical thermodynamic calculation results are basically consistent with the experimental composition. The transition path of inclusions in steel at 1873 K is: $Al_2O_3 \rightarrow YAlO_3 + Al_2O_3 \rightarrow YAlO_3 + Y_2O_2S + YAlO_3 + Al_2O_3 \rightarrow Y_2S_3 + Y_2O_2S$. Y_2S_3 precipitates during the curing process. By increasing the amount of yttrium added, the way to modify Al_2O_3 inclusions in steel is as follows: $Al_2O_3 \rightarrow Y_2S_3 + YAlO_3 + Al_2O_3 \rightarrow Y_2S_3 + YAlO_3 + Y_2O_2S + YAlO_3 + Al_2O_3 \rightarrow Y_2S_3 + Y_2O_2S$.

Acknowledgements No potential conflict of interest was reported by the author(s). This work was financially supported by the National Natural Science Foundation of China (Nos. 51864013 and 52074095). Also, this project supported by National Natural Science Foundation of Guizhou Province with grant No. [2019] 1086.

References

[1] N. Li, L. Wang, Z.L. Xue, C.Z. Li, A. Huang, F.F. Wang, Results Phys. 16 (2020) 102929.
[2] C.F. Yu, Z.L. Xue, W.T. Jin, J. Iron Steel Res. Int. 23 (2016) 338–343.
[3] C.P. Xin, F. Yue, C.X. Jiang, Q.F. Wu, High Temp. Mater. Proc. 35 (2016) 47–54.
[4] D.W. Guo, Z.B. Hou, J.H. Cao, Z.A. Guo, Y. Chang, G.H. Wen, J. Iron Steel Res. Int. 27 (2020) 1163–1170.
[5] L.P. Wu, J.S. Zhang, J.G. Zhi, Q. Liu, C. Su, S.B. Wang, L.L. Zou, Rare Met. Mater. Eng. 49 (2020) 2800–2806.
[6] C.Y. Yang, Y.K. Luan, D.Z. Li, Y.Y. Li, J. Mater. Sci. Technol. 35 (2019) 1298–1308.
[7] H.P. Wang, L. Xiong, L. Zhang, Y. Wang, Y.Y. Shu, Y.H. Zhou, Metall. Mater. Trans. B 48 (2017) 2849–2859.
[8] Z. Adabavazeh, W.S. Hwang, Y.H. Su, Sci. Rep. 7 (2017) 46503.
[9] X.D. Zou, D.P. Zhao, J.C. Sun, C. Wang, H. Matsuura, Metall. Mater. Trans. B 49 (2018) 481–490.
[10] Y. Ren, Y.F. Wang, S.S. Li, L.F. Zhang, X.J. Zuo, S.N. Lekakh, K. Peaslee, Metall. Mater. Trans. B 45 (2014) 1291–1303.
[11] H.T. Ling, L.F. Zhang, JOM 65 (2013) 1155–1163.
[12] X.L. Zhang, S.F. Li, J.S. Yang, J.Q. Wu, Int. J. Miner. Metall. Mater. 27 (2020) 754–763.
[13] Z.G. Wang, C.M. Song, Y.H. Zhang, H. Wang, L. Qi, B. Yang, Mater. Charact. 151 (2019) 112–118.
[14] L. Li, D.Y. Li, J. Phys. Condes. Matter 31 (2019) 1361–1366.
[15] G.X. Qiu, D.P. Zhan, C.S. Li, Y.K. Yang, Z.H. Jiang, H.S. Zhang, Nucl. Eng. Technol. 52 (2019) 811–818.
[16] D.F. Liu, J. Qin, Y.H. Zhang, Z.G. Wang, J.C. Nie, Mater. Sci. Eng. A 797 (2020) 140238.
[17] X.L. Kang, S.Y. Dong, H.B. Wang, S.X. Yan, X.T. Liu, B.S. Xu, Mater. Des. 188 (2020) 108434.
[18] G.J. Cai, Y. Li, Y.R. Huang, R.D.K. Misra, ISIJ Int. 60 (2020) 2541–2548.
[19] S. Gerasin, D. Kalisz, J. Iwanciw, J. Min. Metall. Sect. B Metall. 56 (2019) 11–25.
[20] F. Pan, H.L. Chen, Y.H. Su, Y.H. Su, W.S. Hwang, Sci. Rep. 7 (2017) 2564–2571.
[21] C. Pascal, M. Braccini, V. Parry, E. Fedorova, M. Mantel, D. Oquab, D. Monceau, Mater. Charact. 127 (2017) 161–170.
[22] H.G. Fu, Q. Xiao, J.C. Kuang, Z.Q. Jiang, J.D. Xing, Mater. Sci. Eng. A 466 (2007) 160–165.
[23] J. Yang, D.N. Zou, X.M. Li, Z.Z. Du, J. Iron Steel Res. Int. 14 (2007) 47–52.
[24] H.J. Duan, Y. Zhang, Y. Ren, L.F. Zhang, J. Iron Steel Res. Int. 26 (2019) 962–972.
[25] X.H. Huang, Principles of iron and steel metallurgy, 3rd ed., Metallurgical Industry Press, Beijing, China, 1981.
[26] W.N. Shi, S.F. Yang, J.S. Li, Sci. Rep. 8 (2018) 4830–4839.
[27] C.H. Wu, Study on behavior of inclusions in yttrium-based rare earth microalloyed E36 cast slab, University of Science and Technology Jiangxi, Ganzhou, China, 2016.
[28] Y. Ren, L.F. Zhang, Y. Zhang, J. Iron Steel Res. Int. 25 (2018) 146–156.